Observation of a cubic defect in nickel by means of nuclear magnetic resonance on oriented ^{114}In nuclei

1990 J. Phys.: Condens. Matter 2 1705

(http://iopscience.iop.org/0953-8984/2/7/003)

J. Phys.: Condens. Matter 2 (1990) 1705–1717. Printed in the UK

Observation of a cubic defect in nickel by means of nuclear magnetic resonance on oriented ^{114}In nuclei

A Metz and L Niesen

Laboratorium voor Algemene Natuurkunde, Materials Science Centre, Groningen University, Westersingel 34, 9718 CM Groningen, The Netherlands

Received 18 July 1989

Abstract. ^{114m}In was implanted at room temperature into nickel single crystals, and nuclear magnetic resonance was detected by observing the destruction of β-asymmetry in the decay of ^{114}In. After annealing at 400 K, at which temperature indium atoms are known to trap defects of vacancy-type, two single resonance lines were observed, corresponding to hyperfine fields of $-3.30(1)$ T for the substitutional indium atoms, and $+5.12(2)$ T for the defect associated indium atoms.

The experiments were carried out with an external magnetic field along the ⟨100⟩, ⟨110⟩ and ⟨111⟩ crystallographic axis, respectively. No significant shift or splitting of the defect-associated resonance line was detected. This implies that the defect causes an electric field gradient of at most 10^{17} V cm^{-2}. It is argued that the defect is a cubic vacancy cluster as observed on the system (^{111}In → ^{111}Cd)**Ni** with perturbed angular correlations and Mössbauer spectroscopy on (^{119}In → ^{119}Sn)**Ni**.

1. Introduction

Defect trapping at indium atoms implanted in nickel has been studied extensively by means of perturbed angular correlations (PAC) on ^{111}Cd [1, 2], Mössbauer spectroscopy (MS) on ^{119}Sn [3], and channelling measurements [4, 5]. From these measurements the following picture of defect association in the system **InNi** has emerged. After implantation at room temperature (RT) about 40% of the implanted indium atoms land on substitutional sites. After subsequent annealing at 400 K, at which temperature vacancies are known to become mobile in nickel, approximately 25% of the indium atoms give rise to a well defined defect signal, while the substitutional fraction has decreased to about 20%. The corresponding defect site possesses cubic symmetry and is characterised by a hyperfine field $B_{\rm hf}^{\rm C}$ for the daughter isotopes of $B_{\rm hf}^{\rm C}(^{111}\text{Cd}\mathbf{Ni}) = -2.80(3)$ T, and $B_{\rm hf}^{\rm C}(^{119}\text{Sn}\mathbf{Ni}) = +16.5(2)$ T, respectively.

PAC measurements have revealed two more sites, which are ill defined because the magnetic precession signal is 'smeared-out' as a result of additional quadrupole interactions. Yet another site has been observed only above the Curie temperature of nickel, where it is characterised by an electric field gradient (EFG) of 3×10^{17} V cm^{-2}, which is oriented along a ⟨111⟩ crystallographic axis and has asymmetry parameter $\eta < 0.2$. Whether this defect is also present below the Curie temperature is not clear.

In MS measurements on ^{119}Sn, four additional sites have been found after implantation of ^{119}Xe, which are also proposed to be indium-vacancy complexes. These sites

0953-8984/90/071705 + 13 $03.50

have not been found after implantation of ^{119}In, however. Moreover, due to the small quadrupole moment of the $\frac{3}{2}+$ state in ^{119}Sn, no significant quadrupole interaction could be detected for either of these four sites. Consequently the correspondence with the PAC results is not clear, and the proposed assignments are only tentative.

The cubic site has been interpreted as an interstitial indium atom surrounded by four vacancies. This assignment has been confirmed by ion-channelling results [4] and, even more convincingly by recent electron/positron-channelling measurements [6]. This site is referred to as the C-defect.

The site which possesses ⟨111⟩ symmetry has been interpreted as an indium atom at the centre of planar defect, consisting of at least three vacancies. We will refer to this site as InV_3.

In the present study we have applied nuclear magnetic resonance on oriented nuclei (NMR-ON) to the system In**Ni**. In contrast to the hyperfine interaction methods mentioned above, NMR-ON is sensitive to the environment of the mother nucleus, i.e. the indium itself. This technique has the advantage that it can easily detect a quadrupole splitting of the order of 2 MHz. However, production of sufficient nuclear polarisation is a prerequisite for the observation of NMR-ON, and cooling to temperatures as low as 10 mK is preferable because of rather small hyperfine fields in the system In**Ni**. Substitutional indium in nickel is known to have a hyperfine field of $B_{\mathrm{hf}}^{\mathrm{S}}(\mathrm{In}\mathbf{Ni}) = -3.3$ T [7, 8], and from the values listed above, $B_{\mathrm{hf}}^{\mathrm{C}}(\mathrm{In}\mathbf{Ni})$ is expected to have a value of about +7 T.

2. Nuclear magnetic resonance on oriented nuclei

Before presenting our results we will discuss some general aspects of NMR-ON in ferromagnetic single crystals. Nuclear orientation may be achieved by cooling a sample in an applied magnetic field to a temperature in the millikelvin region. As a result, the angular distribution of the radiation emitted in the radioactive decay of the probe atom becomes anisotropic. A general expression for the resulting angular distribution of the radiation emitted in a certain transition is

$$W(\theta) = \sum_{\lambda} B_\lambda U_\lambda A_\lambda Q_\lambda P_\lambda(\cos\theta) \tag{1}$$

where θ is the angle between the applied magnetic field and the direction of observation, B_λ describes the degree of orientation of the parent level, U_λ accounts for deorientation due to unobserved intermediate transitions, A_λ describes the anisotropy of the observed transition, Q_λ is a correction factor that accounts for the finite solid angle subtended by the detector, and P_λ is a Legendre polynomial. For γ-radiation, the sum in equation (1) contains only even terms, whereas for β-radiation also odd terms are included, which results in an asymmetric distribution. At high temperatures $W(\theta) = 1$, irrespective of θ. The decay of ^{114}In proceeds via an allowed Gamow–Teller transition, in which case only terms up to $\lambda = 1$ occur in (1) and the angular distribution is given by

$$W_{\beta^-}(\theta) = 1 + B_1 A_1^{\beta^-} Q_1 P_1(\cos\theta) \tag{2}$$

with

$$A_1^{\beta^-} = -\sqrt{\tfrac{2}{3}}(v/c).$$

When the magnetic field at the site of the radioactive nucleus is positive, the β-asymmetry $W_{\beta^-}(0) - 1$ is also positive.

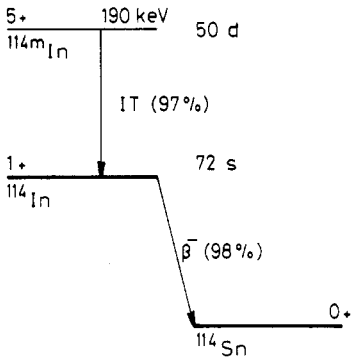

Figure 1. Simplified decay scheme of the ^{114}In isomers.

In figure 1 a simplified decay scheme of the ^{114}In isomeric states is shown. The long-lived ^{114m}In decays via a 190 keV γ-transition to the short-lived ground state, which decays by β-emission to ^{114}Sn. When 40% of the indium atoms experience a hyperfine field of -3 T at a temperature of 10 mK, one calculates for the 190 keV transition: $W_\gamma(0) = 0.98$ and $W_\gamma(\pi/2) = 1.01$. For the β-asymmetry a much larger effect is calculated: $W_{\beta^-}(0) = 0.79$. Consequently we focused our attention on this quantity.

In practice, the observed β-asymmetry is often reduced. In the first place the β-radiation is focused by the polarising field, so that the effective opening angle of the detector is increased. In a strong magnetic field $\boldsymbol{Q}_1$ will be reduced to 0.5. Loss of asymmetry is also caused by scattering of the β-particles. Finally, radioactive self-heating, which is estimated to be 35 nW for a source strength of 0.5 MBq, may lead to an increase in the temperature of the source with respect to the surroundings.

In an NMR experiment, transitions between the spin levels are induced by a transverse radio-frequency (RF) field, which results in a destruction of asymmetry when the RF matches the energy-splitting of the nuclear spin system. In the case of a purely magnetic interaction, the relation between the resonance frequency ν_m and the hyperfine field B_{hf} is given by:

$$h\nu_m = g_n\mu_n[B_{hf} + (1 + K)(B_{app} - \mu_0 N_{zz} M_s)]. \tag{3}$$

Here, g_n and μ_n are the nuclear g-factor and magneton, respectively. K is the Knight shift, B_{app} is the applied magnetic field, and the term $\mu_0 N_{zz} M_s$ represent the demagnetising field, which is determined by the shape of the sample through the tensor $\mathbf{N}$.

When an additional quadrupole interaction is present, as will be the case when the ^{114}In atom is associated with a non-cubic defect cluster, the resonance line splits up into a large number of components, the frequency of which depends on the angle between B_{app} and the main axis of the EFG; however, this was not observed in the present experiments. If the additional quadrupole interaction is small with respect to the magnetic interaction, $2I$ components result for a given orientation of the EFG. When we consider only the transition between the lowest two spin levels, which is dominant at low temperatures, the following expression for the resonance frequency ν results:

$$h\nu = h\nu_m - (3eQV_{zz}/4I)\{P_2(\cos\theta) + \tfrac{1}{2}\eta \sin^2\theta \cos 2\varphi\}. \tag{4}$$

Here Q is the quadrupole moment, V_{zz} is the main component of the electric field gradient tensor, η is the asymmetry parameter and the Euler angles θ and φ define the orientation of the EFG principal axes with respect to the applied field. For an arbitrary

combination (θ, φ, η), 24 equivalent orientations exist in a cubic lattice. A study of the line splitting for different orientations of the magnetic field may, in principle, reveal the orientation of the EFG [9, 10].

Because the resonance lines in ferromagnetic materials are inhomogeneously broadened, the resonance signal can only be detected when the RF signal is frequency modulated (FM). Conventionally, both FM on and FM off counts are collected. We define the resonance signal $S(\nu)$ as

$$S(\nu) = W_{\mathrm{FMoff}}(\nu) - W_{\mathrm{FMon}}(\nu) = [N_{\mathrm{FMoff}}(\nu) - N_{\mathrm{FMon}}(\nu)]/N_{\mathrm{warm}} \tag{5}$$

where N_{warm} is the count rate at relatively high temperature, where no β-asymmetry is present. In this way we may eliminate a possible frequency dependence of the non-resonant count rate. The area of a resonance line with resonance frequency ν_i, divided by the frequency modulation width $\Delta\nu_{\mathrm{FM}}$, which we will denote by $S^{\mathrm{I}}(\nu_i)$, is a measure of the total amount of β-asymmetry that is destroyed in this resonance

$$S^{\mathrm{I}}(\nu_i) = \int S(\nu)\,\mathrm{d}\nu/\Delta\nu_{\mathrm{FM}}. \tag{6}$$

The total fraction of nuclei f_i that contributes to a given resonance ν_i, can be obtained by dividing the destruction of assymetry $S^{\mathrm{I}}(\nu_i)$ by the calculated β-asymmetry $W^{\mathrm{calc}}_{\beta^-}(\nu_i, T) - 1$, where T is the temperature during the measurement

$$f_i = S^{\mathrm{I}}(\nu_i)/[W^{\mathrm{calc}}_{\beta^-}(\nu_i, T) - 1]. \tag{7}$$

We would like to stress the fact that it is of crucial importance to use the calculated value W_{calc}, rather than the commonly used experimental value W_{exp}, when the total observed asymmetry consists of different contributions with opposite sign, as is the case in the present experiment.

In practice, the observed fractions f_i will not add up to one, even not if all resonances have actually been found, because of the reduction of the observed β-asymmetry as discussed above. Moreover, complete destruction of asymmetry can only be achieved when the resonance is saturated, and this was not always the case under the present experimental conditions.

With respect to the last point, the magnetisation behaviour of the single crystals is of importance. The number of NMR-ON experiments carried out on nickel single crystals is surprisingly small, and a study of the magnetisation behaviour of nickel single crystals by means of nuclear orientation, has not been reported in the literature. We conclude this section with a qualitative discussion of the magnetisation behaviour of nickel at low temperatures.

In order to maximise the observable asymmetry, it is necessary to align the magnetic domains, thus creating one single domain. The magnetic field required to achieve this depends on its orientation with respect to the cubic crystallographic axes. In the case of nickel, the $\langle 100\rangle$-axis is a magnetically 'hard' axis, whereas the $\langle 111\rangle$-axis is an 'easy' axis. This phenomenon is quantitatively described by the magneto-crystalline anisotropy energy E_{a}, which is given by the following expression for a cubic crystal:

$$E_{\mathrm{a}} = K_0 + K_1(\alpha_1^2\alpha_2^2 + \alpha_2^2\alpha_3^2 + \alpha_3^2\alpha_1^2) + K_2\alpha_1^2\alpha_2^2\alpha_3^2 + \ldots \tag{8}$$

where the α_i are the directional cosines of the magnetisation with respect to the cubic crystallographic axes. The ellipsis indicates higher order terms, which may *not* be neglected for an accurate description of the magnetisation of nickel at low temperatures [11, 12]. In the present discussion we will only consider the anisotropy constants K_1 and

Table 1. Sample dimensions and calculated demagnetising and anisotropy fields. The saturation field B_{sat} equals the sum of B_a and $\mu_0 M_s N_{zz}$. For the saturation magnetisation $\mu_0 M_s$ a value of 640 mT is used.

Sample	Dimensions (mm)	Demagnetising factors			Demagnetising field, $\mu_0 M_s N_{zz}$ (mT)	Anisotropy field, B_a (mT)
		N_{xx}	N_{yy}	N_{zz}		
⟨100⟩	1.0 × 4.0 × 9.5	0.768	0.179	0.053	34	$-2K_1/M_s = 484$
⟨110⟩	1.0 × 3.7 × 11.0	0.763	0.196	0.041	26	$-(K_1 + 0.5\,K_2)/M_s = 191$
⟨111⟩	1.0 × 3.8 × 11.8	0.769	0.193	0.038	24	0

K_2, whose values are given by Franse and de Vries [12] as $K_1 = -1.234 \times 10^5$ J m^{-3} and $K_2 = 0.521 \times 10^5$ J m^{-3} at 4 K. These constants determine the field B_{sat} required to rotate the magnetisation parallel to the direction of the applied field, when the field is oriented along a ⟨100⟩ or ⟨110⟩ crystallographic axis. B_{sat} is the sum of the anisotropy field B_a and the demagnetising field $\mu_0 N_{zz} M_s$. When the field is applied along a ⟨111⟩ direction, B_a is zero, and B_{sat} equals the demagnetising field $\mu_0 N_{zz} M_s$. The values of B_a and $\mu_0 N_{zz} M_s$ for these three cases are listed in table 1.

When NMR experiments are carried out on ferromagnetic materials, it is usually observed that the NMR-signal decreases when the applied magnetic field is increased. This is the result of the fact that the so-called 'hyperfine enhancement factor' decreases with increasing field. In an NMR-ON experiment one therefore expects the largest signal when B_{app} equals B_{sat}.

3. Experimental procedure

Three nickel single crystals of 99.999% purity were cut with their long axes approximately parallel to the ⟨100⟩, ⟨110⟩ and ⟨111⟩ crystallographic axes, respectively. The sample dimensions and the diagonal elements of the demagnetising tensor **N** are included in table 1. In order to increase the β count rate, the crystal surfaces were tilted by 5° with respect to the direction of the applied magnetic field. The crystallographic axes were tilted with respect to the crystal surfaces by the same angle, so that the magnetic field could be applied exactly along the desired axis. The coordinate system used to define the orientation of the samples, is shown in figure 2; the relation between this system and the crystallographic axes is given in table 2.

The samples were mechanically polished and electrochemically etched using a mixture of 10 ml H_3PO_4 (85%), 4 ml H_2O and 1 ml H_2SO_4 (100%). Thereafter they were soldered with indium on silver sample holders. Before implantation, the crystals were etched again, to remove a possible contaminating layer from the surface that may have developed during the soldering process.

^{114m}In was produced by neutron irradiation of indium of 99.9999% purity. It was implanted into the crystals at room temperature. During all implantations, the total dose was approximately ten times the radioactive dose. A well known contaminant with mass 114 is MoO [13]; however, replacement of Mo materials in the ion source by Ta did not lead to a reduction of the contamination.

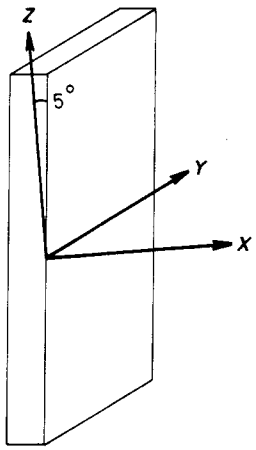

Figure 2. Orientation of the single crystals. The magnetic field is applied along **Z**. The orientation of the axes can be found in table 2.

Table 2. Orientation of the single crystals. For the choice of the coordinate system refer to figure 2.

Sample	*X*	*Y*	*Z*
⟨100⟩	⟨01$\bar{1}$⟩	⟨011⟩	⟨100⟩
⟨110⟩	⟨1$\bar{1}$0⟩	⟨00$\bar{1}$⟩	⟨110⟩
⟨111⟩	⟨1$\bar{1}$0⟩	⟨112⟩	⟨111⟩

A conventional dilution refrigerator with a base temperature of 14 mK was used to precool a $PrNi_5$ nuclear cooling stage in an initial field of 2.5 T. For the NMR-ON measurements described here a high cooling power at temperatures around 8 mK is more important than a low base temperature. Therefore the final field on the $PrNi_5$ stage was normally chosen as 0.4 T, leading to a base temperature of 5 mK. The sample holders could be inserted into the cold finger by means of a top loading system. The temperature of the sample holder was determined with a ^{54}MnNi nuclear orientation thermometer, that was soldered onto the sample holder with eutectic GaIn, which has a melting point of 18 °C. This solder was used to avoid unintended annealing of the implanted samples.

The radiative destruction of asymmetry was observed on the 0.7 to 2 MeV region of the β-spectrum of ^{114}In, by means of a Si detector mounted inside the cryostat. This detector had to be heated to 60 K to operate properly, and was shielded from the sample by means of an aluminised mylar foil, which was cooled to 1.5 K. NMR-ON measurements were performed by sweeping the RF up and down through the frequency region of interest, collecting counts at each frequency point during 60 s, while switching the frequency modulation alternatively on and off. Data collection was interrupted for 5 s after FM_{off} and 10 s after FM_{on} counting periods, to allow for spin-lattice relaxation. The choice of these times is based upon a spin lattice relaxation time of 8 s, which was measured by Magendans [8] on a nickel foil at 20 mK. NMR-ON searches were carried out at temperatures of about 20 mK, using the dilution refrigerator only. Using the $PrNi_5$ stage, more accurate NMR-ON spectra were recorded. During these measurements the temperature of the $PrNi_5$ stage typically increased from 8 mK to 10 mK.

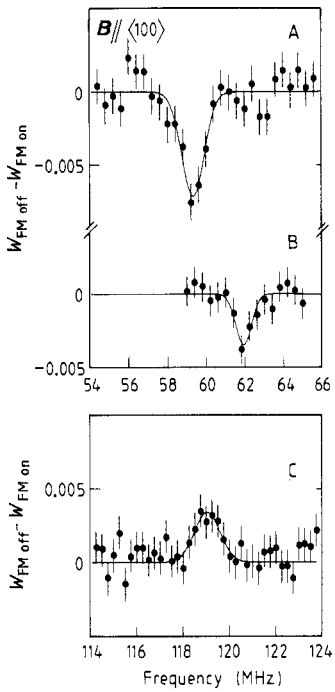

Figure 3. NMR-ON spectra for the ⟨100⟩ orientation. Curve A, as implanted, and measured in a field of 552 mT at 23 mK; curve B, annealed at 400 K, and measured in a field of 437 mT at 29 mK; curve C, annealed at 400 K, and measured in a field of 437 mT at 16 mK.

Attempts to observe the γ-anisotropy of the 190 keV line in the decay of ^{114m}In were hampered by a background of Compton scattered γ-radiation from the decay of ^{54}Mn. Moreover, in the vertical direction, the 190 keV γ-intensity was severely attenuated by the mass of the β-detector. In addition, the theoretical γ-anisotropy is rather small. Our measurements of the γ-anisotropy suffered from very poor statistics, and will not be reported here.

4. Results

4.1. ⟨100⟩-orientation

The ⟨100⟩ crystal was implanted at RT with 110 keV ^{114m}In ions to a dose of 1×10^{14} atoms cm^{-2}. A radioactive source of 0.75 MBq was obtained, with a maximum impurity concentration of 130 ppm at a depth of 20 nm. After cooling to 5 mK in an applied field of 552 mT, the β-asymmetry $W_{\beta-}(0) - 1$ was -0.04. In spite of the surprisingly small value, a NMR-ON search was carried out for the substitutional resonance at a temperature of 23 mK. A well defined resonance signal was detected as shown in figure 3, curve A. Here, as in all subsequent NMR-ON spectra, the resonance signal $S(\nu)$ as defined in equation (5), is plotted as a function of the frequency ν. The sign of the resonance signal is sensitive to the sign of the magnetic field at the site of the nucleus, and is negative for negative magnetic fields. The centre frequency was determined as 59.32(9) MHz by fitting a Gaussian curve to the resonance line. Two additional substitutional resonances were recorded for an external field of 437 mT and 320 mT, respectively. At the lowest field, the resonance signal was clearly reduced, and we

conclude that the magnetisation is close to saturation at 437 mT, which is in reasonable agreement with the value of B_{sat} given in table 1. A search for defect-associated frequencies was carried out at 20 mK, in the frequency region 20–180 MHz, but no significant signal was found.

After annealing the sample in vacuum at 400 K for 30 min and subsequent cooling to 8 mK in an applied field of 437 mT, the β-asymmetry $W_{\beta-}(0) - 1$ was +0.06. This is a clear indication that now an increased number of the implanted ^{114}In nuclei were experiencing a positive hyperfine field. The presence of two hyperfine fields of opposite sign also gives a good explanation of the small values of the observed β-asymmetry, which is the net result of two contributions of opposite sign and comparable magnitude.

During the subsequent NMR-ON measurements, the thermal contact between the sample holder and the cold finger was rather poor. The substitutional resonance was recorded at a temperature of 29 mK, and is shown in figure 3, curve B. The shift with respect to figure 3, curve A is caused by a change in the external field. As a result of the annealing the substitutional fraction is reduced by a factor of 2. An NMR-ON search for additional resonances was carried out with a modulation width of 1.6 MHz at temperatures around 25 mK, in the frequency region from 20 to 300 MHz. We found a weak resonance signal at 119 MHz. It was measured again with a modulation width of 0.5 MHz at a temperature of 16 mK, and is shown in figure 3, curve C. This resonance corresponds to a positive hyperfine field, as can be inferred from the sign of the resonance signal.

4.2. ⟨110⟩-orientation

The ⟨110⟩ crystal was implanted at RT with 110 keV ^{114m}In ions to a dose of 1.5×10^{14} atoms cm^{-2}. A radioactive source of 0.50 MBq was obtained with a maximum impurity concentration of 200 ppm at a depth of 20 nm. After cooling to a temperature of 10 mK in an applied field of 175 mT, the β-asymmetry $W_{\beta-}(0) - 1$ was −0.02. In this experiment all NMR-ON measurements were carried out at a temperature of about 10 mK, and the field dependence of the substitutional resonance could easily be studied. The resonance signal attained its largest value at 200 mT, in good agreement with the value of B_{sat} listed in table 1. In figure 4, curve A the substitutional resonance, recorded at an applied field of 175 mT is shown. In figure 5 we show the variation of the substitutional resonance with the applied field. From a least-squares fit to the data we determined $d\nu/dB_{app} = -21.4(4)$ MHz T^{-1}. Neglecting a possible Knight shift, we obtain a value of 2.81(5) μ_n for the magnetic moment of ^{114}In, which is in good agreement with the reported value of 2.816(5) μ_n [14].

After annealing at 400 K in vacuum for 30 min, and subsequent cooling to 6 mK in an applied field of 175 mT, the β-asymmetry $W_{\beta-}(0) - 1$ was +0.05. In this field the defect-associated resonance was found at the expected frequency of 113 MHz, as shown in figure 4, curve B. Again the substitutional fraction was observed to decrease by a factor of 2 as a result of the annealing.

4.3. ⟨111⟩-orientation

The ⟨111⟩ crystal was implanted at RT with 110 keV ^{114m}In ions to a dose of 1.5×10^{14} atoms cm^{-2}. A radioactive source of 0.75 MBq was obtained with a maximum impurity concentration of 200 ppm at a depth of 20 nm. After cooling to a temperature of 10 mK in an applied field of 117 mT, no significant β-asymmetry could be detected.

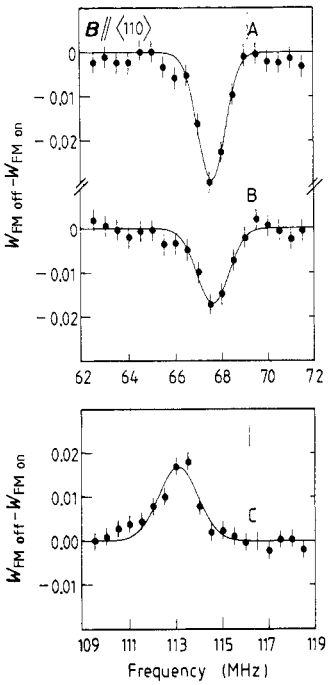

Figure 4. NMR-ON spectra for the ⟨110⟩ orientation. Curve A, as implanted; curves B and C, annealed at 400 K. The applied field was 175 mT in all cases, and the measurements were carried out at a temperature of approximately 10 mK.

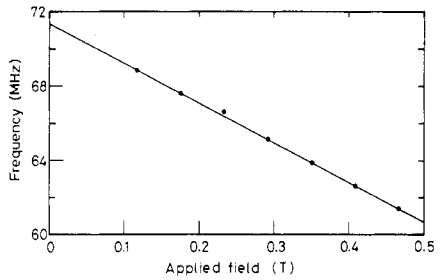

Figure 5. Variation of the resonance frequency with the applied magnetic field. NMR-ON spectra were recorded at 10 mK, with $\boldsymbol{B} \parallel \langle 110 \rangle$. Full circles, experimental data; full line, least-squares fit with slope $d\nu/dB_{app} = -21.4(4)$ MHz T^{-1}. The statistical errors are about the size of the full circles.

Initial NMR-ON measurements on the substitutional resonance, at an external field of 58 mT and 117 mT, respectively, both yielded very poor results. In figure 6, curve A we show the substitutional resonance that we obtained at an external field of 117 mT, after increasing the RF power by a factor of 3 with respect to the measurements on the other crystals. A possible explanation for these small effects is that at a temperature of 10 mK, at which the measurements were carried out, the spin lattice relaxation for the ⟨111⟩ orientation is so slow that the short-lived ^{114}In ground state does not reach thermal equilibrium.

After annealing at 400 K in vacuum for 30 min and subsequent cooling to 5 mK in an applied field of 117 mT, the β-asymmetry $W_{\beta-}(0) - 1$ was +0.03. In this field the defect associated resonance was found at the expected frequency of 112 MHz. As for the two cases reported above, we observed a decrease of the substitutional fraction by a factor of 2, approximately. The NMR-ON spectra for these cases are shown in figure 6.

5. Discussion

5.1. Zero-field resonance frequencies

In table 3 we present a summary of the calculated zero field frequencies. Tentative values for the site populations are listed in table 4, and the observed linewidths are listed in

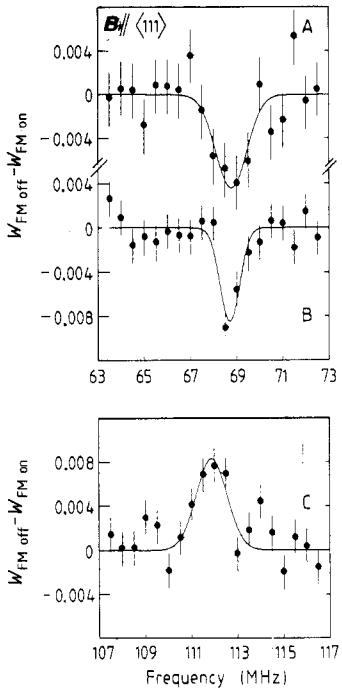

Figure 6. NMR-ON spectra for the ⟨111⟩ orientation. Curve A, as implanted; curves B and C, annealed at 400 K. The applied field was 117 mT in all cases, and the measurements were carried out at a temperature of approximately 10 mK.

Table 3. Extrapolated zero field frequencies as obtained from a least-squares fit with a single Gaussian curve. All values are in MHz.

	As implanted	Annealed at 400 K	
Sample	Substitutional resonance	Substitutional resonance	Defect-associated resonance
⟨100⟩	70.43(24)	70.58(21)	110.39(21)
⟨110⟩	70.79(10)	70.81(13)	109.90(13)
⟨111⟩	70.77(18)	70.70(11)†	109.88(16)

† Linewidth fixed.

table 5. The extrapolation to zero field was done by using the measured value of $d\nu/dB_{app}$ as reported in § 4.2 above, and applying a correction for the demagnetising field. The values used for N_{zz} are listed in table 1. From the average zero field frequencies and the reported value for the magnetic moment of ^{114}In [14], we obtain the following hyperfine fields:

$$B_{hf}^{S}(^{114}\mathbf{InNi}) = -3.30(1)\ \mathrm{T} \qquad B_{hf}^{C}(^{114}\mathbf{InNi}) = +5.12(2)\ \mathrm{T}.$$

The value for the substitutional hyperfine field agrees perfectly with the value reported by Kontani and Itoh [7].

Table 4. Tentative site populations as obtained from a least-squares fit with a single Gaussian curve.

	As implanted	Annealed at 400 K	
Sample	Substitutional resonance	Substitutional resonance	Defect-associated resonance
⟨100⟩	0.15(2)	0.06(2)	0.05(1)
⟨110⟩	0.18(1)	0.10(1)	0.14(1)
⟨111⟩	0.05(2)	0.03(1)†	0.06(2)

† Linewidth fixed.

Table 5. Resonance linewidths (FWHM) as obtained from a least-squares fit with a single Gaussian curve. The modulation width $\Delta\nu_{FM}$ is included in the table. All values are in MHZ.

	As implanted		Annealed at 400 K			
	Substitutional resonance		Substitutional resonance		Defect-associated resonance	
Sample	FWHM	$\Delta\nu_{FM}$	FWHM	$\Delta\nu_{FM}$	FWHM	$\Delta\nu_{FM}$
⟨100⟩	1.4(2)	0.8	0.9(3)	0.8	1.3(3)	0.5
⟨110⟩	1.4(1)	1.0	1.6(2)	1.0	2.0(2)	1.0
⟨111⟩	1.6(4)	1.0	1.0†	1.0	1.6(3)	1.0

† Linewidth fixed.

5.2. Site populations

The tentative site populations for the ⟨111⟩ crystal are smaller by a factor of 2 than the corresponding values for the other orientations. A similar reduction was observed for the β-asymmetry (cf §§ 4.1 to 4.3). The spin-lattice relaxation in ferromagnetic single crystals is known to be slowest when a magnetic field is applied along an 'easy' axis. We attribute, therefore, the small effects in the case of the ⟨111⟩ orientation to the fact that the ^{114}In ground state does not reach thermal equilibrium with the lattice during its lifetime of 72 s.

Even in the case of the ⟨110⟩ orientation, for which the largest effects were observed, there is a discrepancy between the fractions as derived from the PAC measurements and our results. As already noted in § 2, this may be the result of either insufficient RF power, or loss of β-asymmetry. Nevertheless, in each series of measurements for a single orientation, relative changes of site occupation can be inferred from the reported values.

The reduction of the substitutional fraction after annealing at 400 K is in good agreement with the PAC and MS results. Evidence for an increase of the defect associated fraction is given by the fact that in all three cases positive hyperfine fields dominate the β-assymetry after annealing, whereas before annealing the β-asymmetry was found to be zero or negative. The existence of other fractions, with either sign of hyperfine field, cannot be excluded.

5.3. Resonance linewidths

The statistical accuracy of our results does not allow us to give a detailed discussion of the resonance lineshapes. The majority of the observed resonances, as listed in table 5, has a linewidth which is significantly larger than the modulation width. Therefore we did not correct our values for the effect of frequency modulation. The linewidths are typically 1.5 MHz, which is quite normal for implanted systems.

Of great interest is the question as to whether an EFG is associated with the defect resonance. Unfortunately, the quadrupole moment of ^{114}In is not known. The most accurate results for the quadrupole moments of the corresponding spin 1 states in ^{112}In and ^{116}In are 0.093 and 0.09 b, respectively [15], and we will tentatively assume $Q(^{114}\text{In}) = 0.09$ b.

A general discussion including all possible EFG orientations would be quite complicated, as may be seen from equation (4). We will, therefore, focus our attention on an EFG with a $\langle 111 \rangle$ orientation and $\eta = 0$, as was found in the PAC measurements. In this case one expects for $\boldsymbol{B} \parallel \langle 110 \rangle$ a splitting in two lines of equal amplitude, separated by

$$\Delta\nu = 3eQV_{zz}/4hI. \tag{9}$$

We fitted two Gaussian curves with a fixed frequency splitting to the defect associated resonance line for $\boldsymbol{B} \parallel \langle 100 \rangle$ (figure 4, curve C). For a splitting of 2 MHz the normalised χ^2 increased from 1.0 to 2.7, which implies that such a splitting can be safely ruled out. An EFG with the above mentioned symmetry is therefore limited to a value of 10^{17} V cm^{-2}. Since the Sternheimer anti-shielding factors for indium and cadmium differ by only 10% [16], this can be directly compared to the value of 3×10^{17} V cm^{-2} that was obtained for the InV_3 defect by means of PAC. We conclude therefore, that the defect associated resonance observed in our NMR-ON measurements is not due to the InV_3 defect.

5.4. Interpretation of the defect-associated resonance

The absence of a marked quadrupole splitting is the strongest argument to assign the observed defect-associated resonance line to the C-defect that was observed in PAC-measurements. This point of view is in accordance with the annealing behaviour, as discussed in § 5.2. Moreover, also in the PAC experiments on ^{111}In and probably also in the MS experiments on ^{119}In the dominant defect fraction is associated with the cubic defect.

In figure 7 we plotted the hyperfine fields for the substitutional and cubic defect sites, for the elements Cd, In and Sn. The value of the defect associated hyperfine field for ^{114}In**Ni**, fits well with the trend of hyperfine fields of C-defects.

The variation of the hyperfine fields with atomic number can be understood from the work of Kanamori and co-workers [17]. The central point in their interpretation is the splitting of the impurity s-states in bonding orbitals which give a negative contribution to the hyperfine field, and anti-bonding orbitals which give a variable contribution that depends on their position with respect to the Fermi level. With increasing atomic number Z the impurity potential becomes deeper, so that the antibonding orbitals shift to lower energies, and the hyperfine field increases. When the distance between the impurity atom and the neighbouring host atoms is increased, as is the case for the C-defect, the mixing between impurity s orbitals and host d orbitals decreases. This effect leads to a smaller splitting between the bonding and the antibonding orbitals, so that the latter are

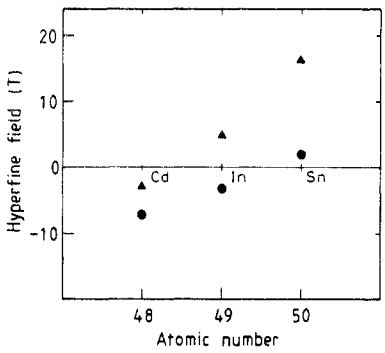

Figure 7. Variation of the hyperfine field with atomic number. Full circles, substitutional defect; full triangles, C defect.

pulled down with respect to the Fermi level, which results in an increase of the impurity hyperfine field.

The experimental data show that B_{hf}^{C} increases much faster with Z than B_{hf}^{S}. This effect cannot easily be explained by means of the 'hand-waving' arguments used above. Further theoretical effort is required to elucidate this point.

Acknowledgments

The authors are grateful to A H J Timans for maintenance of the cryogenic equipment, F Th. ten Broek for radiochemical assistance, J J Smit for carrying out the implantations and L Venema for preparation of the single crystals.

This work was performed as part of the research program of the Stichting voor Fundamenteel Onderzoek der Materie (FOM) with financial support from the Nederlandse Organisatie voor Wetenschappelijk Onderzoek (NWO).

References

[1] Hohenemser C, Arends A R, de Waard H, Devare H G, Pleiter F and Drentje S A 1977 *Hyperfine Interact.* **3** 297
[2] Allard C, Collins G S and Hohenemser C 1985 *Phys. Rev.* B **32** 4839
[3] Nielsen K Bonde, Danielsen E, Petersen J W, Söndergaard M and Weyer G 1987 *Hyperfine Interact.* **35** 643
[4] Howe L M, Swanson M L and Quenneville A F 1983 *Nucl. Instrum. Methods* **218** 663
[5] Vos M, Boerma D O and Pleiter F 1986 *Nucl. Instrum. Methods* B **15** 333
[6] Hofsäss H, Lindner G, Winter S and Recknagel E 1988 *Nuclear Physics Applications on Materials Science* ed. E Recknagel and J C Soares (Dordrecht: Kluwer) p 157
[7] Kontani M and Itoh J 1967 *J. Phys. Soc. Japan* **22** 345
[8] Magendans F C, University of Groningen, unpublished results
[9] Visser D, Niesen L, Postma H and de Waard H 1978 *Phys. Rev. Lett.* **41** 882
[10] Metz A and Niesen L 1989 *Phys. Rev.* B **39** 2029
[11] Aubert G, Ayant Y, Belorizky E and Casalegno R 1976 *Phys. Rev.* B **14** 5314
[12] Franse J J M and de Vries G 1968 *Physica* **39** 477
[13] Lattimer W W and Stone N J 1979 *Hyperfine Interact.* **7** 61
[14] Nuytten C, Vandeplassche D, van Walle E and Vanneste L 1982 *Phys. Rev.* C **26** 1701
[15] Lederer C M and Shirley V S (ed.) 1978 *Table of Isotopes* 7th edn (New York: Wiley)
[16] Feiock F D and Johnson W R 1969 *Phys. Rev.* **187** 39
[17] Kanamori J, Yoshida H K and Terakura K 1981 *Hyperfine Interact.* **9** 363